ceramics

MDPI

Review

The Role of Sacrificial and/or Protective Layers to Improve the Sintering of Electroactive Ceramics: Application to Piezoelectric PZT-Printed Thick Films for MEMS

Hélène Debéda [1,*], Maria-Isabel Rua-Taborda [1,2], Onuma Santawitee [1], Simon Grall [1], Mario Maglione [2], U-Chan Chung [2] and Catherine Elissalde [2]

[1] Laboratoire IMS, Université de Bordeaux, UMR 5218, 33405 Talence, France; isabel.rua.t@gmail.com (M.-I.R.-T.); onuma.santawitee@u-bordeaux.fr (O.S.); simon.grall@mail.com (S.G.)

[2] CNRS, Université de Bordeaux, ICMCB, UMR-5026, 33600 Talence, France; mario.maglione@icmcb.cnrs.fr (M.M.); u-chan.chung@icmcb.cnrs.fr (U.-C.C.); catherine.elissalde@icmcb.cnrs.fr (C.E.)

* Correspondence: helene.debeda@ims-bordeaux.fr; Tel.: +33-5-4000-8336

Received: 11 August 2020; Accepted: 20 October 2020; Published: 16 November 2020

Abstract: Piezoelectric thick films are of real interest for devices such as ceramic Micro-ElectroMechanical Systems (MEMS) because they bridge the gap between thin films and bulk ceramics. The basic design of MEMS includes electrodes, a functional material, and a substrate, and efforts are currently focused on simplified processes. In this respect, screen-printing combined with a sacrificial layer approach is attractive due to its low cost and the wide range of targeted materials. Both the role and the nature of the sacrificial layer, usually a carbon or mineral type, depend on the process and the final device. First, a sacrificial layer method dedicated to screen-printed thick-film ceramic and LTCC MEMS is presented. Second, the recent processing of piezoelectric thick-film ceramic MEMS using spark plasma sintering combined with a protective layer approach is introduced. Whatever the approach, the focus is on the interdependent effects of the microstructure, chemistry, and strain/stress, which need to be controlled to ensure reliable and performant properties of the multilayer electroceramics. Here the goal is to highlight the benefits and the large perspectives of using sacrificial/protective layers, with an emphasis on the pros and cons of such a strategy when targeting a complex piezoelectric MEMS design.

Keywords: sacrificial layer; protective layer; thick film; screen-printing; spark plasma sintering; piezoelectric; carbonate

1. Introduction

In the world of applications based on MEMS (Micro-ElectroMechanical Systems), the use of a piezoelectric material with direct and/or inverse effects is of real interest for sensing, actuating, energy harvesting, or Structural Health Monitoring applications [1]. MEMS classification depends on the nature of the substrate, so ceramic, silicon, and organic MEMS are all discussed. According to the type of MEMS, specific fabrication techniques are required. In silicon MEMS, for example, either bulk or surface micromachining is used to achieve free-standing layers [2]. These processes require numerous and quite complicated fabrication steps. For each instance of micromachining, humid, or dry etching is the final process stage leading to movable microstructures. Considering sacrificial surface silicon micromachining, the microstructure is fabricated on top of both a silicon substrate and a sacrificial thin film whose thickness determines the final gap between the substrate and the mechanical structure.

In the case of bulk micromachining, the microsystem is fabricated from the silicon wafer thanks to an etching process of the exposed silicon regions. It is important to point out here that in silicon piezoelectric MEMS, the integrated piezoelectric layers are mainly thin films of AlN, ZnO, or PZT [3]. Nevertheless, for specific applications that require a higher volume of active material, thick films are of real interest because they bridge the gap between thin films and bulk ceramics. Today, different processing routes such as 3D printing, ink-jet, sol-gel, and aerosol are considered to shape thick films with thicknesses in the range 1–100 µm [4,5]. Among them, the screen-printing technology, widely used in microelectronics and more recently in flexible electronics, appears to be an attractive technique due to its simplicity, low cost, and wide range of targeted materials. For instance, silicon bulk micromachining technology associated with screen-printing $Pb(ZrTi)O_3$ (PZT) was successfully developed for preparing micropumps, actuators, accelerometers, and energy harvesters [6]. However, MEMS processing had to be improved and adapted to overcome issues such as the Pb diffusion towards silicon with the formation of lead silicate compounds, the incompatibilities with standard silicon wet etching, and the fragility of the mechanical silicon structure due to the pressure applied by the squeegee during printing. The use of a sacrificial layer is easy to implement in MEMS processing and has allowed one to optimize the process with a reduction in the number of fabrication steps. Its role depends on the targeted device and is thus adapted to the process. In the case of ceramic MEMS, the sacrificial layer allows one to partially remove a ceramic layer from its substrate leading to free standing structures. This method based on a carbon type sacrificial layer was introduced in the early 1980s to develop the first ceramic MEMS for pressure sensors based on screen-printed thick films [7,8]. Carbon or mineral type sacrificial layers were also considered for releasing in the late 2000s for screen-printed PZT MEMS with different geometries [9,10]. The use of the sacrificial layer approach was also considered at that time for manufacturing LTCC (low-temperature co-fired ceramic) ceramic MEMS [11] to overcome the collapse of the structures or cavities during hot rolling and/or final firing. The nature of the sacrificial layer is obviously related to the type of MEMS (Si, organic, or ceramics) and to the active layer that is subsequently released [12–14].

In this paper, LTTC ceramics MEMS that use green tape to structure the active ceramic layer and thick-film ceramic MEMS based on screen-printed layers are considered.

The first part is devoted to a survey of literature highlighting three main types of sacrificial layers whose removal during or at the end of the process will depend on their composition. Particular emphasis will then be paid to the processing by conventional sintering of PZT-based thick-film MEMS and their characteristics. It will be shown that, according to the active piezoelectric material and the required conventional thermal treatment, both the nature of the sacrificial layer and the releasing approach will have an impact on the chemistry, the microstructure, and strain/stress issues. Controlling the whole process and selecting the relevant materials are crucial for the properties of the printed piezoelectric thick-film MEMS.

In the second part of this paper, original approaches targeting bulk ceramic and thick-film ceramic MEMS produced using advanced sintering techniques associated with protective layers are introduced. While sacrificial materials have already been shown to act as a pore forming agent or as a thermal or diffusion barrier for bulk ceramics [15,16], carbonate based protective materials have recently appeared to efficiently prevent PZT from chemical reduction during spark plasma sintering (SPS) [17]. Chemistry, microstructure, and stress/strain effects are again issues strongly linked to sintering and whose control has an impact on the performance of the electroactive multilayer. An approach combining SPS and a protective layer is illustrated based on our recent investigations on PZT thick-film ceramic MEMS with an emphasis on the pros and cons of such a strategy targeting a complex MEMS design.

Finally, we conclude with the challenges and opportunities of eco-friendly approaches aiming a global improvement in processing in the field of electroactive ceramic MEMS.

2. Sacrificial Layers for LTCC and Thick-Film Ceramic MEMS

Considering ceramic MEMS, two technologies can be found: Screen-printing of thick-film ceramic MEMS and LTCC ceramic MEMS. In thick-film ceramic MEMS, the ceramic, mainly alumina, is used as a support for the structural layers, whereas in LTCC, green tapes formed from alumina and glass powders are the support for the integration of further active or passive layers. The different approaches used for surface micromachining of such ceramic MEMS are detailed in the following paragraphs.

2.1. LTCC Ceramic MEMS

For the processing of LTCC ceramic MEMS, three types of sacrificial layers are reported [11,18]: A carbon-based sacrificial layer burnt out during the sintering process and two mineral compositions, a glass and a carbonate-based sacrificial layer. Both of them need removal after the firing process.

2.1.1. Carbon Approach

In the carbon approach, the carbon-based sacrificial layer is eliminated during the firing process by oxidation. Here, sagging of the cavities has to be controlled thanks to an optimized sintering profile and a fine control of the air/nitrogen ratio, leading to a gasification of the carbon while the carbon is oxidized (Figure 1a). This approach was considered by Birol et al. [19], who used a graphite-based sacrificial layer in the manufacturing of ceramic microfluidic microstructures and sensors. The authors pointed out the complexity of the process and that it depends on the specifications of the final device: The dimensions and the mechanical and functional properties. In particular, the influence of the composition of the sacrificial layer, the carbon powder grain size, and the heat treatment on the geometrical characteristics (sagging, delamination, swelling, etc.) of the fired microstructure was highlighted. This study also raised the problem of microstructural warpage related to the departure of the carbon products, which must take place before the complete elimination of the ceramic porosity. Capacitive pressure sensors based on LTCC materials were also prepared by Dai et al. [20] in which the role of the sacrificial layer nature and the thermal treatment to properly evacuate the combustion products were underlined. This kind of sensor, with an inductor and a capacitor was composed of four green tapes stacked together before their co-sintering at 900 °C, (Figure 1b). As shown before, a polyimide or carbon sacrificial layer was also introduced into the multilayer and removed during firing to create a cavity between the two capacitors plates and to ensure a good flatness of the top electrode. Contrarily to the carbon layer, the polyimide layer dimensions had to be adapted to take into account the coefficient of thermal expansion coefficient (CTE) mismatch with the tape material. Experiments carried out with and without air evacuation channels showed that, despite the presence of the air channel, residues of polyimide are still found in the cavity because of its relatively high decomposition temperature (≈600 °C), at which the LTCC tape was already too dense. Interestingly, when using the carbon sacrificial layer, carbon oxidation could be controlled with carbon dioxide evacuation through the porous ceramic before its final densification (Figure 1b). Thus, in this case, the use of a vent channel and its further sealing would no longer be necessary.

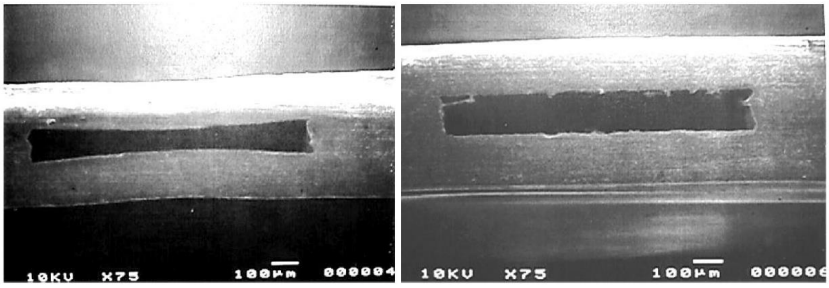

(**a**)

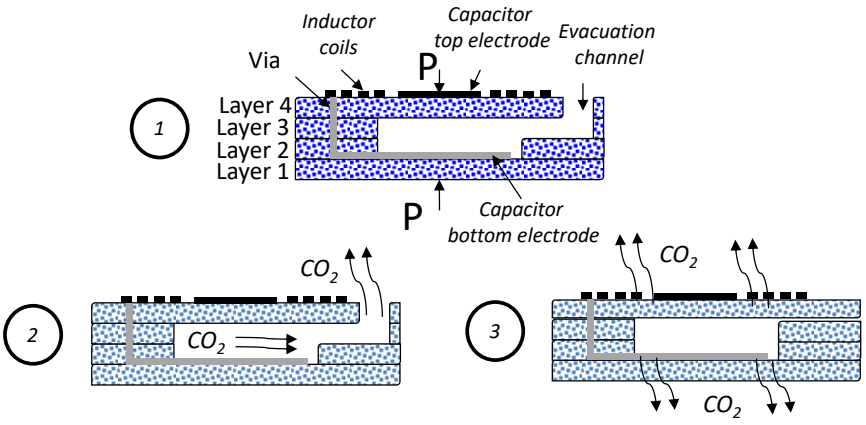

(**b**)

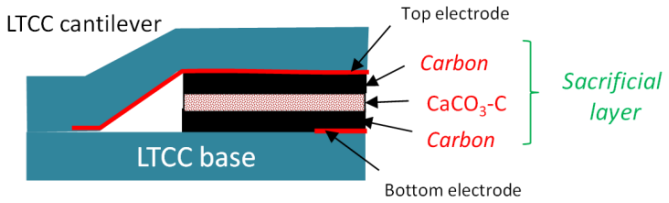

(**c**)

Figure 1. LTCC (low-temperature co-fired ceramic) ceramic Micro-ElectroMechanical Systems (MEMS). (**a**) Photograph of a cavity after sintering without (left) and with carbon black paste (right) reproduced with permission from [11] copyright 2001 Elsevier. (**b**) Scheme of a pressure sensor inspired from Dai et al. [20]: 1. Principle; 2. CO_2 evacuation during the sintering through the dedicated channel or 3. Through the porosity. (**c**) Scheme of a cantilever force sensor (capacitive principle) fabricated using a sandwich sacrificial layer (inspired from Fournier et al. [21]).

2.1.2. Mineral Approach

In the mineral approach, the glass-type sacrificial layer (PbO-SiO_2 glass frit system) is removed by a hydrofluoric acid solution at the end of the process. Nevertheless, the etching rate inside the cavities is very low, with limited solubility in the lead silicate glass frit. Another drawback is that the etching rate is comparable to that of the ceramic tapes of similar composition.

Mixtures of mineral-based sacrificial layer easily removable in a weak acid or base solution were also explored by Birol et al. and Fournier et al. [19,21]. The sacrificial pastes were based on oxide mixtures (CaO-H_3BO_3, CaO-B_2O_3, and CaO-$Na_2B_4O_7$). The authors also reported sacrificial pastes based on carbonates, i.e., a mix of carbon and calcium carbonate. Similar to the study reported by Lucat et al. [22], the sacrificial layer based on $CaCO_3$ with carbon (28 wt% $CaCO_3$ + 72 wt% C) showed the best results (good gap quality and no LTCC deformation). An LTCC capacitive anemometer was

successfully fabricated with this process by using a sacrificial layer composed by the stacking of three layers made of CaCO3_C and sandwiched between top and bottom pure carbon layers (Figure 1c).

The approach with a carbonate-based mineral sacrificial layer, partially decomposed during the thermal treatment and for which the remaining carbonate was etched at the end of the process, was first initiated by Lucat et al. in their investigation on thick-film ceramic MEMS [22,23]. Different types of thick-film ceramics, including PZT MEMS performed using an epoxy matrix loaded with $SrCO_3$ as a sacrificial layer, have been reported, and are illustrated in the following section.

2.2. Thick-Film Ceramic MEMS

2.2.1. Carbon Approach

G. Stecher et al. at Bosch Gmbh were pioneers in the patented work related to the manufacturing of sensors in classical thick-film technology with the use of a carbon sacrificial layer [7,8].

This process of manufacturing a capacitive or piezoresistive pressure sensor by screen printing is potentially exploitable for the realization of closed-cavity structures and can be described by the following steps (Figure 2a): The deposition and the thermal treatment of a carbon filled polymer ink, which acts as a sacrificial layer; the deposition of a glass-ceramic type dielectric that acts as a porous structural layer and that is partially covering the substrate and completely overlaying the sacrificial layer; firing under nitrogen in order to not oxidize the sacrificial layer while consolidating the structural layer; firing the component under air to remove the sacrificial carbon layer through the porosity of the structural layer; the deposition of a vitreous structural layer on the porous dielectric layer in order to seal and mechanically reinforce the latter; the deposition of additional structural layers to functionalize the sensor; and air firing to consolidate the sensor.

The first application resulting from this process was the fabrication of a pressure sensor using a cavity formed by the substrate and an impermeable circular membrane on which four Wheatstone bridge piezoresistors were screen-printed.

At the end of the 2000s, Kok et al. also investigated the possibility of using piezoelectric cantilevers for energy harvesting [13]. In this work, as in Birol et al.'s work [19] on LTTC ceramic MEMS, the sacrificial layer was a screen-printed carbon layer that burnt out above 800 °C. Very recently, other options of a sacrificial layer based on polyester or on epoxy loaded with corn starch were studied by Santawitee et al. and Grall et al. [24,25]. These sacrificial layers were fully removed during the sintering of the structural layers; as a result, highly densified piezoelectric cantilevers or disk types were obtained. A difference in the thermal decomposition of these two new sacrificial layers (Figure 3) was shown to influence the PZT sintering with higher densification in the case of the corn-starch-based sacrificial layers, which have a higher decomposition temperature.

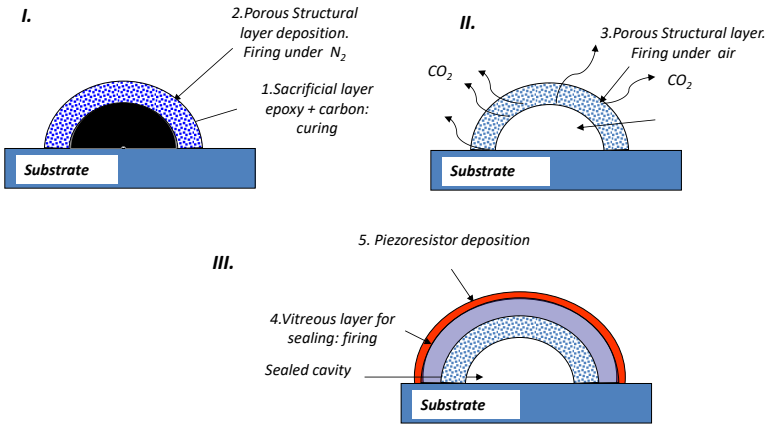

(**a**)

Figure 2. *Cont.*

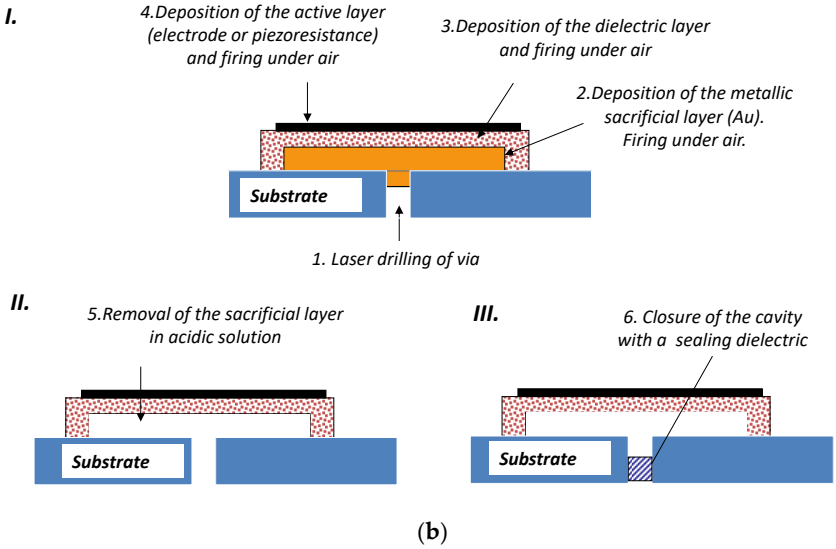

(**b**)

Figure 2. Example of manufacturing steps of thick-film ceramic MEMS pressure sensors using two sacrificial layer compositions: (**a**) Epoxy + carbon and (**b**) gold (inspired respectively from [8] and [26]).

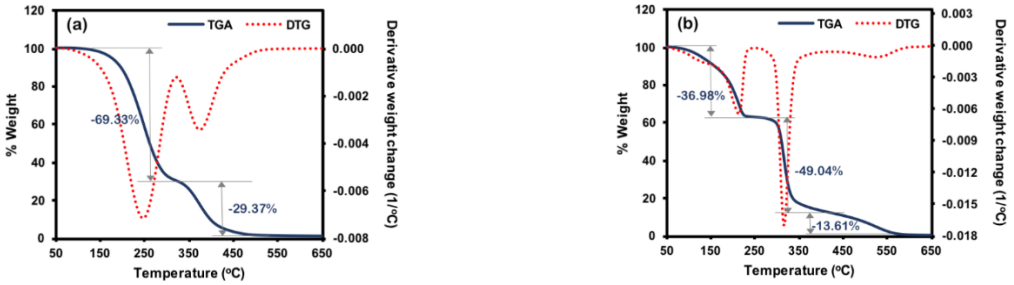

(**a**) (**b**)

Figure 3. TGA and DTG of (**a**) polyester and (**b**) epoxy-corn starch sacrificial layers used for piezoelectric thick-film ceramic MEMS fabrication.

2.2.2. Mineral Approach

Nearly 20 years after Stecher's work, Sippola et al. [26] implemented a process for manufacturing pressure sensors, also based on the sacrificial layer approach, but while considering the use of a non-carbon sacrificial layer. This sensor was a sealed cavity formed by a dielectric membrane screen-printed on an alumina substrate. This hermetic volume was obtained by screen-printing the dielectric layer on a sacrificial gold layer, which was previously deposited on the alumina substrate and then removed by an acid solution through an aperture made in the substrate (Figure 2b).

In the middle of 2000, Lucat et al. proposed to replace the carbon, metal, and glass phases by a mineral carbonate in order to simplify the process [22,23]. In this new process, the sacrificial layer was an epoxy resin filled with strontium carbonate powder. The main criteria in the choice of the carbonate mineral part contained in the sacrificial layer were as follows: Its ease of elimination at the end of the process in a weak acid or base solution and its physico–chemical stability (reactivity, melting point, etc.) during heat treatment.

Moreover, as a base for screen-printing paste, the authors opted for the thermosetting epoxy resin offering the best compromise between the following: Good chemical compatibility with other materials; ease of application by screen-printing and enough stiffness to support the following deposit of layers; and temperature resistance.

Thanks to the use of this epoxy-strontium carbonate composite ink, electrothermal copper microactuators were successfully developed for the first time in 2007 [27]. The process was also

applied to manufacture partially detached components from the substrate that are not intended to be actuated, e.g., metal alloy resistors for heating sensors or 3D microstructures such as microchannels (Figure 4a,b). In addition, the flexibility of this process made it possible to produce piezoresistive cantilever force sensors [28] and piezoelectric components, partially or completely released from the substrate for sensing, actuating, or Structural Health Monitoring [29–31]. For all these applications, the sintering of the structural layers took place between 850 and 900 °C, while thermal decomposition of the epoxy polymer base was achieved at 550 °C. The strontium carbonate included in the sacrificial paste remained stable up to these temperatures and was then soluble at the end of the process in a weak acidic solution (phosphoric acid H_3PO_4) following the reaction:

$$MCO_{3(s)} + 2H_3O^+ \leftrightarrow M^{2+} + CO_{2(g)} + 3H_2O \quad (1)$$

SEM analysis of a cross-section of a silver microchannel showed the efficiency of the process [22]. Nevertheless, chemical reactivity between the glass and carbonate was noticed in the case of a glass microchannel, as illustrated by the Castaing microprobe analysis of an unreleased microchannel (Figure 4c). This chemical reactivity was reduced by adding 5% CO_2 to the firing atmosphere, leading to a decrease in the thickness of the interface (about 3 µm) (Figure 4d).

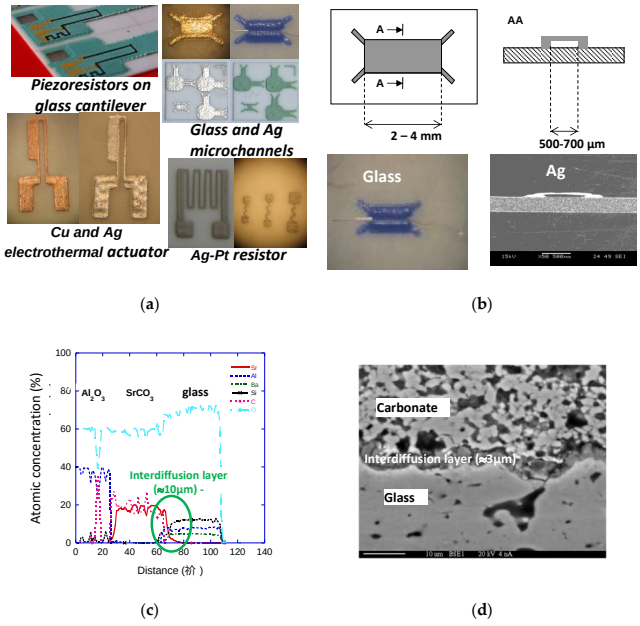

Figure 4. Thick-film ceramic MEMS associating screen-printing with an $SrCO_3$-epoxy sacrificial layer. (**a**) Photographs of successfully fabricated microstructures. (**b**) Dimensions, photograph, and SEM images of microchannels. (**c**,**d**) Interface glass/$SrCO_3$ analysis revealing the presence of strontium: (**c**) Castaing microprobe analysis after firing under air of the cross section of the interface glass/$SrCO_3$; (**d**) SEM image after firing under air + 5% CO_2 [32].

To sum up, three main types of sacrificial layer compositions can be identified from a survey of literature focused on thick films and LTTC ceramic MEMS: A glass- or metal-based composition that will be chemically dissolved in a solution of strong acid or base at the end of the process, as in silicon technology (this process requires selective etching to avoid attacking the structural layers); a composite or all-organic composition based on carbon, corn starch, or polyester that is consumed during sintering and thus bypasses the problem of removing the sacrificial layer at the end of the process; and a mineral composition based on carbonate, presenting good compatibility with most of the structural layers and easily removable at the end of the process with a weak acid.

Using these sacrificial-layer-based processes, the applications target microfluidic, sensing, actuating, or energy harvesting. Some aspects of the fabrication process (sintering temperature, active

material, sacrificial layer nature, and its removal) are given in Table 1 for each of the above-mentioned ceramic MEMS examples (LTCC and thick-film type). It should be emphasized that, in the last decades, PZT in thick-film architecture was mainly studied as an electroactive material because of its outstanding properties and the wide range of potential applications. As a result, the following section is focused on the processing and properties of the PZT-based thick-film ceramics.

Table 1. Key process-related characteristics distinguishing ceramic MEMS using the sacrificial layer process and corresponding applications (TF = thick-film and LTCC = low-temperature co-fired ceramics) [7–9,19–22,24–30,33–36].

Ceramic MEMS Type/Multilayer Nature	T_{Sint}	Sacrificial Layer Nature/Elimination	Applications	Ref/Year
TF	-	Polymer + carbon	Pressure sensor	[7] 1984 [8] 1987
LTCC/ glass-ceramic	850 °C	Carbon black/burnt out	Cavity	[33] 1998
LTCC/ glass-ceramic	-	Lead-silicate/etching in buffered hydrofluoric acid	Suspended bridging structure, cavity	[33] 1998
TF/electrode/dielectric	-	Au	Pressure sensor	[26] 2005
TF/Ag	450 °C	Registration paste carbon ink/burnt out	Microwave inductor	[34] 2005
LTCC	875 °C	Epoxy + carbon/burnt out	Pressure sensor + microfluidic	[19] 2006
LTTC/ AgPd	875 °C	Carbon + $CaCO_3$/burnt out + $CaCO_3$ etching in phosphoric acid	Capacitive anemometer	[21] 2007
TF/ AgPd/PZT/AgPd	850–950 °C	Epoxy + carbon/burnt out	Energy harvester	[9] 2009
TF/ Au, Cu, Ag, glass, piezoresistor on glass, Au/PZT/Au	850–900 °C	Epoxy + $SrCO_3$/epoxy burnt out+ $SrCO_3$ etching in phosphoric acid	Thermal actuator, force sensor, microchannels, microresistors, piezoelectric transducers (gas detection, SHM)	[22] 2008 [27] 2007 [28] 2010 [29] 2013 [30] 2014 [35] 2016
LTCC/ piezoresistor	>700 °C	Epoxy + carbon or Polyimide/burnt out	Pressure sensor	[20] 2015
TF/Au/PZT/Au or AgPd/PZT/AgPd	900 °C	Polyester/burnt out	Piezoelectric cantilever and disk (mass sensing, cantilever sensors,)	[36] 2019 [24] 2020
TF/ Au/PZT/Au	900 °C	Epoxy + corn starch/burnt out	Piezoelectric disks and cantilever	[25] 2020

2.3. PZT Thick-Film Ceramic MEMS

In this section, since some studies have already reported PZT screen-printing on silicon [37,38] followed by its release, only thick films printed on ceramic substrates and partially or completely dissociated from the substrate are considered. Bounded screen-printed PZT layers can be found in the literature [39–42], and more recently lead-free piezoelectric layers [43]; however, to the best of our knowledge, only screen-printed PZT thick films have been released from the substrate. When processing screen-printed PZT thick films using a conventional process, the PZT layers contain a residual porosity. When the sintering temperature is increased above 950 °C, PZT's stoechiometry can be modified if the atmosphere is not controlled to prevent Pb losses. Interdiffusion phenomena between the layers during co-sintering can also affect the properties. As a result, the use of a sintering aid, associated to an isostatic pressing step was the selected option to improve densification while reducing the sintering temperature [44,45]. Here, and according to the classification discussed above, we will classify the used sacrificial layers in two categories according to the removal step:

- Mineral $SrCO_3$-based sacrificial layers etched at the end of the process.
- Carbon-based or all organic sacrificial layers removed during the sintering.

2.3.1. Mineral Approach

In the mineral approach, the $SrCO_3$ is mixed with epoxy to confer consistency to the screen-printable ink. The microstructure of a free-standing PZT layer in a sandwich architecture between two Au electrodes supporting the fragile piezoceramic layer can be compared to multilayers sintered on alumina and stainless steel substrates (SS), respectively (Figure 5a,b). Au electrode and PZT layers are successively printed, dried at 120 °C between each step, and the stacked layers are finally co-sintered. All the layers are isostatically pressed at 40 MPa before sintering. $Li_2CO_3Bi_2O_3CuO$ (LBCu) was successfully used as a sintering aid to reduce the sintering temperature to 900 °C while keeping good piezoelectric properties, as reported in [46]. The addition of only 3% in weight of LBCu was shown to be efficient for PZT sintering, both the melting of the binary system Bi_2O_3-Li_2CO_3 and the presence of CuO play a significant role in lowering the sintering temperature [47,48]. For bounded layers, a diffusion/adhesion layer is formed between the substrate and the Au layer, as already observed in [40,42]. In the case of the free-standing PZT layer, only a slight diffusion of Sr into the Au layer is observed, showing the efficiency of the Au electrode as a barrier to limit PZT/$SrCO_3$ cross-diffusion (Figure 5c). The densification of bounded and free standing layers evaluated by ImageJ [36] is quite similar, with a porosity of 20–25%. This residual porosity is the consequence of the densification being affected by the mechanical clamping of the substrates on one side, and by the constrained shrinkage on the remaining $SrCO_3$ during the sintering on the other.

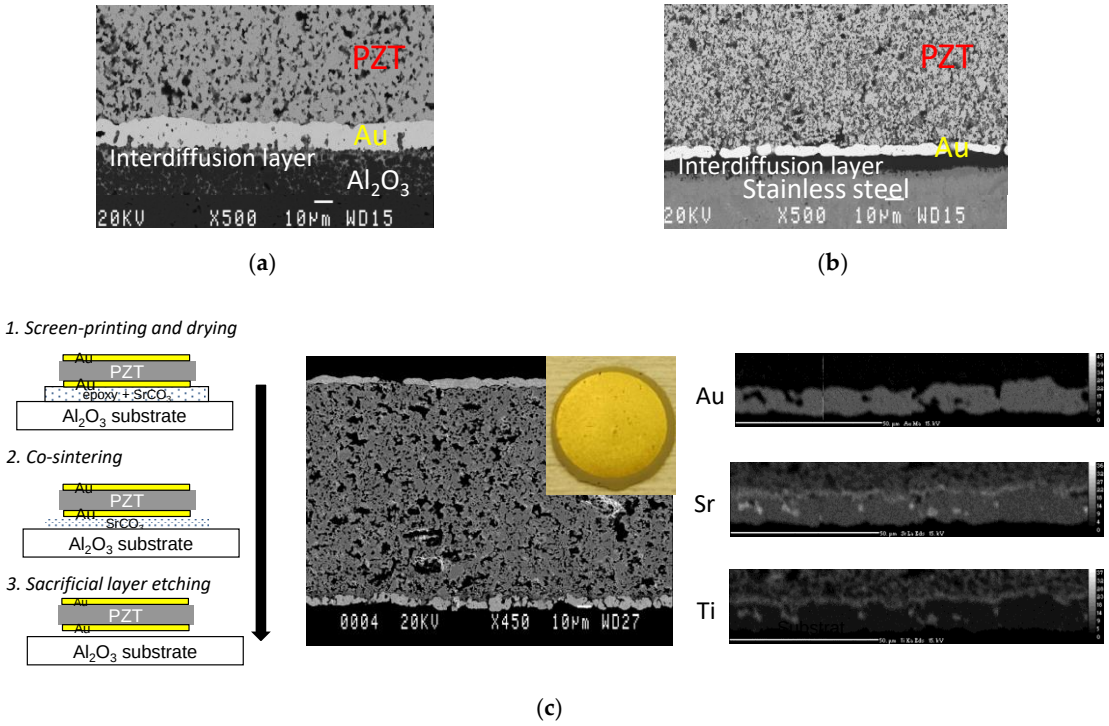

Figure 5. Comparison of SEM microstructures of PZT + LBCu screen-printed layers sintered on different supports (alumina substrate, stainless steel substrate, or epoxy + $SrCO_3$). (**a**) Au/PZT/Au on alumina substrate. (**b**) Au/PZT/Au on stainless steel substrate (SS301). (**c**) Totally released Au/PZT/Au disks after deposition on epoxy + $SrCO_3$ sacrificial layer and acidic dissolution in phosphoric acid. (left) Fabrication steps; (middle) SEM of a microsection; (right) Castaing micropobe analysis at the PZT/bottom electrode interface adapted with permission from [30] copyright 2014 Wiley

2.3.2. Carbon Approach

In the carbon approach, the sacrificial layers are burnt during the sintering under air. Kok et al. [9,49] reported a piezoelectric energy harvester based on free-standing PZT cantilevers (9 mm wide, 4.5 to 18 mm long, ≈90 µm thick) for which a graphite sacrificial layer is used, as in LTCC ceramic MEMS [19l]. Here, because of the important thermal expansion coefficient's mismatch between the AgPd electrodes and the sandwiched PZT, additional thin uniform layers of non-active PZT (unpoled) (≈10 µm) were hence printed on both sides of the cantilever to prevent delamination and warpage (Figure 6a,b). All layers were co-fired in air at a temperature higher than 850 °C and the sacrificial carbon layer was burnt out at the same time with a shrinkage of about 10%. Finally, the device showed improved performances with better piezoelectric coefficient d_{33} for the sintering temperature of 950 °C, but more cracks were noticed compared to the sintering performed at 850 °C.

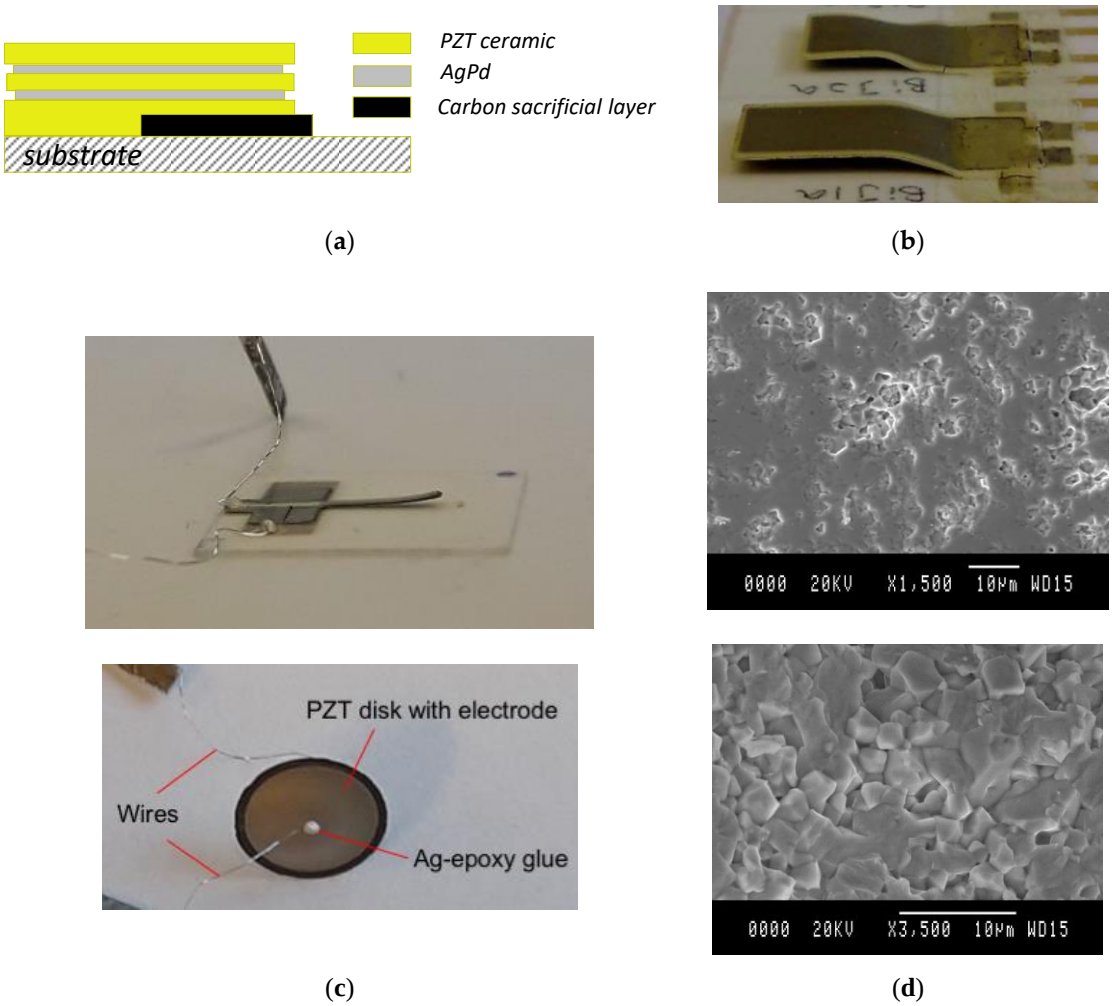

Figure 6. Photographs and SEM images of PZT free-standing devices. (**a**) Assembly scheme (inspired from [49]) (**b**) photograph of a free-standing cantilever (carbon sacrificial layer). Reproduced with permission from [9], copyright 2009 IOP. (**c**) Au/PZT/Au cantilever and AgPd/PZT/AgPd disks (polyester sacrificial layer). (**d**) SEM images of PZT printed on a polyester sacrificial layer: Upper image: Polished cross section; lower image: Fractured ceramic

More recently, Grall et al. and Santawitee et al. [24,36] used a polyester sacrificial layer and successfully released PZT disks and cantilevers, while obtaining density values close to those of bulk ceramics. In this case, considering a cantilever of dimensions $8 \times 2 \times 0.1$ mm^2, made of PZT with LBCu as a sintering aid and Au electrodes, a typical shrinkage of 13% was obtained after firing at 900 °C. Moreover, with the same sintering conditions but with a disk shape, changing the electrode from Au to AgPd led to enhanced piezoelectric properties. This gain in performance was associated with a better quality of interface between the AgPd electrode and PZT, because of the presence of the $MgTiO_3$ additive in the electrode helping to adjust the CTE of the electrode [24]. Photographs and SEM images of PZT free-standing thick films components developed by Kok et al., Santawitee et al., and Grall et al. [24,36,49] are shown in Figure 6. These images reveal curvatures and porosity-related oissues that have to be overcome during the shaping and conventional sintering (T < 900 °C) of piezoelectric screen-printed multilayers.

Piezoelectric transducer geometries chosen according to application can be simple disks, bridges, or cantilevers. Their properties are compared in Table 2 to those of a commercial hard type PZT in bulk (PZ26) or thick-film form (TF2100). The dielectric and piezoelectric properties are clearly correlated to the density, PZT sintering aid, electrode, and sacrificial layer material choices. Disks fired on polyester or corn starch present a higher density value (>7000 kg/m^3). Thanks to improved densities, the relative permittivity is higher than 600 and can even reach 1200 when using both AgPd electrodes and a polyester sacrificial layer. These properties are clearly improved compared to those of the TF2100 thick films sintered on alumina.

To sum up, the microstructures of PZT thick-film layers depend on the nature of the supporting layer and/or on the substrate on which they are sintered. In addition to the influence of sintering conditions and as illustrated in Figure 7, lateral shrinkage can also be improved by adapting the sacrificial layer nature [24,25,30].

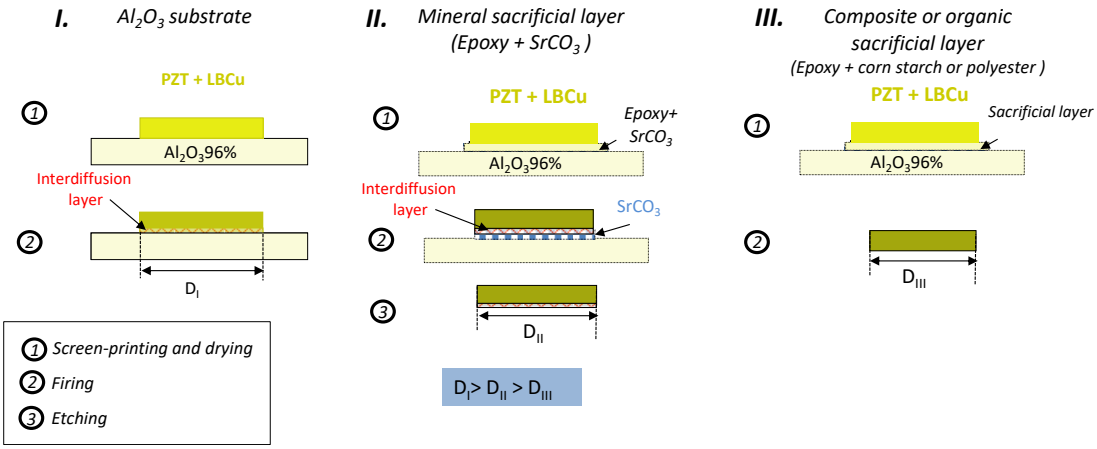

Figure 7. Simplified scheme showing phenomena occurring during the PZT + LBCu sintering of screen-printed thick films (disk shape) on a mineral or organic type sacrificial layer. D is the final diameter of the disk cross-section.

Table 2. Comparison of the properties of PZT films used in thick-film ceramic MEMS [9,24,25,30,31,40,42,46,49–51].

Supporting Substrate (S) or Sacrificial Layer (SL) for PZT Printing	Geometry/PZT Thickness	Multi-Layer/PZT Type	Sintering Aid and Sintering Temperature	Density (kg/m^3)	Relative Permittivity ε_{33} (1 kHz, RT [1]	$-d_{31}/d_{33}$ (pC/N)	Ref/Year
SL epoxy + $SrCO_3$/	Bridge 5 mm × 3.3 mm/80 µm	Au/PZT/Au (PZT [2])	5 wt % glass [3]/850 °C	5500	150	-	[31] 2015
SL epoxy + $SrCO_3$/	Cantilever 8mm × 2 mm/100 µm	Au/PZT/Au (PZ26 [4])	5 wt % glass [3]/900 °C	5500	340	90	[46] 2014
SL Carbon	Cantilever 18 mm × 9 mm 90 µm	PZT/AgPd/PZT/AgPd/PZT (PZ29 [4])	4 wt % glass [3]/850 °C–950 °C	-	336 617	−20/53 −28/80	[49] 2014 [9] 2009
SL epoxy + $SrCO_3$	Disk	Au/PZT/Au (PZ26 [4])	3 wt % LBCu /900 °C	5200	630	−40/-	[30] 2014
SL Polyester	Disk ⌀ 7.74 /100 µm	Au/PZT/Au (PZ26 [4])	3 wt % LBCu /900 °C	7400	600	−121/-	[42] 2020
SL Polyester	Disk ⌀ 7.5 mm /140 µm	AgPd/PZT/AgPd (PZ26 [4])	3 wt % LBCu/900 °C	7400	1200	-	[24] 2020
SL epoxy + Corn-starch	Disk ⌀ 7.5 Cantilever 2 mm × 1 mm/100 µm	PZT Au/PZT/Au (PZ26 [4])	3 wt % LBCu /900 °C	7500 7200	-	-	[25] 2020
Thick-film TF1200 Insensor A/S	-	PZ26 [4]	sintering aid/850 °C [40]	5000	520	−50/200	[50] 2012
Commercial bulk Ferroperm	-	PZ26 [4]	-/>1200 °C	7800	1300	−130/330	[51] 2007

[1] RT = Room Temperature; [2] PZT synthetized by the solid phase method; [3] Lead borosilicate glass; [4] PZ26 = hard relaxor PZT (Navy I) and PZ29 = traditional soft PZT.

3. Protective Layers Combined with Spark Plasma Sintering: Bulk Ceramics and Thick-Film Ceramic MEMS

As mentioned in the previous section, thick-film ceramic performances are strongly linked to strain issues and microstructural features. For most piezoelectric ceramics, the sintering temperature ($T_{sint.}$) is critical because, when too high, secondary phases, interdiffusion, non-stoichiometry, the volatility of elements, and the lack of grain size control are hardly avoidable drawbacks. Properties including electrical conductivity, piezoelectric strain and charge, and ferroelectric switching are all strongly dependent on defect chemistry and microstructure. When considering conventional sintering, several strategies aim to optimize sintering conditions. Among them and as recalled previously, sintering aids such as LBCu, $LiBiO_2$ + CuO [47] or Li_2CO_3 + PbO [52] can allow one to efficiently lower the sintering temperature below 1000 °C. However, the level of porosity, close to 20%, remains to be improved. The control of the sintering atmosphere is also crucial for lead-based piezoelectric compositions. The quite low melting point of lead oxide is an issue that can cause unwanted changes in stoichiometry and thus in properties. In conventional sintering, green samples are generally placed on top of sacrificial powders used to protect the sample from any chemical interaction with aluminum oxide crucibles and/or to maintain a sufficiently high vapor pressure of PbO. A PbO or $PbZrO_3$ sacrificial powder bed ensures the lead-rich atmosphere required to prevent PbO losses [53]. An alternative powder bed consisting of ZrO_2 sand reacted with PbO was found to sufficiently reduce the PbO loss in PZT compositions avoiding secondary phases. In addition, such a sacrificial mixture can be easily removed from both the samples and the crucible after sintering [54].

The use of advanced sintering processes is another approach to optimize PZT densification at low temperature. PZT ceramics were recently sintered at 300 °C by a Cold Sintering Process using bimodal powders and $Pb(NO_3)_2$ as a sintering aid. The relative density and functional properties were improved after a post annealing performed at 900 °C [55]. The advantages of spark plasma sintering (SPS) in terms of enhanced sintering kinetics (combined action of pressure and electric current) were also explored to obtain dense PZT ceramics in a shorter time and at a lower sintering temperature compared to conventional sintering. A literature survey shows that PZT and related solid solutions are sintered by SPS under low oxygen partial pressure at temperatures close to or higher than 900 °C without any sintering aid in most cases. However, a post-annealing treatment is systematically performed under air and in the range 700–1100 °C to remove oxygen vacancies and associated charged defects that contribute to the conductivity and can alter the poling process [56].

3.1. Sacrificial/Protective Materials Approaches Combined with Spark Plasma Sintering

In order to efficiently use SPS at temperatures not higher than 900 °C and in one step, the challenge is to manage the thermal and chemical gradients arising from both fast kinetics and a low oxygen partial pressure environment.

Both the heat conduction and current pathway will influence the chemistry and the microstructure [57]. Thermal and electrical barriers using insulating disks or thermal buffers during SPS were reported in the literature. These allow one to reduce the heat conduction and to control the current distribution across punch/die/powder assembly (limited current leakage). They can be located either directly in contact with the powder or between the rams and punches [58]. Alumina powders were also used to prevent ferroelectric ceramics from chemical reduction during SPS [16] and to prevent the pistons of the deforming copper spiral extremities in the co-sintering of transformers for power electronics [59]. Alumina powder placed on both sides of ZnO samples were also used to insulate ZnO from the current. Insulation prevents the influence of the electric field on the ZnO grains, which affects the reactivity and diffusion during sintering [60]. Also noteworthy is the innovative approach based on sacrificial Al_2O_3 or ZrO_2 powders reported by C. Manière et al. to fabricate complex shape materials with a controlled microstructure. The corresponding deformed interface method includes the assembly, the sintering, and the removal of sacrificial parts [61,62].

Here we focus on the use of carbonates as a protective powder layer targeting the one-step SPS of PZT at a low temperature without sintering aids and avoiding an additional step of post-annealing treatment. As mentioned in Section 2.3, $SrCO_3$ was already successfully used as a sacrificial layer to perform the released screen-printed piezoelectric disk or cantilevers [30]. Carbonates fulfill the multiple criteria required to target not only ceramic but also screen-printed MEMS. The protective layer placed on top of the PZT is expected to protect it from chemical reduction under a low oxygen partial pressure environment, to be inert at the selected sintering temperature, to discard the chemical interaction with the different layers (PZT, electrodes, and metallic substrate), and to be easily removed by polishing or etching after sintering. Considering the decomposition temperature of some carbonates, $SrCO_3$ and $BaCO_3$ (the latter of which has an even higher decomposition temperature) were selected as protective layers (Table 3).

Table 3. Decomposition temperature of carbonates.

Carbonate	Decomposition Temperature (°C)
$MgCO_3$	350
$CaCO_3$	850
$SrCO_3$	1100
$BaCO_3$	1740

In the next section, the efficiency of $SrCO_3$ and $BaCO_3$ protective layers is first demonstrated and compared in the case of SPS of PZT ceramics. The microstructure, dielectric, and electromechanical properties of the as-obtained PZT ceramics are compared to those of the PZT processed by conventional sintering and by SPS in classical conditions without a protective layer. Afterward, it is shown that this strategy was adapted to the sintering of screen-printed multilayers for MEMS applications.

3.2. Carbonates as a Protective Layer for PZT Bulk Ceramics by SPS

Sintering was performed using an SPS apparatus Syntex Inc., SPS-515S. The PZT powder without a sintering aid was loaded in a cylindrical graphite die with an inner diameter of 10 mm and heated under a low oxygen partial pressure. The temperature was raised at 50 °C/min and kept at a constant value at 875 °C for 5 min. A pressure of 100 MPa was applied along the *Z*-axis of the graphite die during the whole sintering process. When no protective layers were used, the samples were annealed in air at 800 °C for 10 h in order to remove surface carbon contamination and to limit oxygen vacancies caused by the reducing conditions. When protective layers were used, the carbonate powders were deposited on the bottom and on the top of the PZT. The sintering cycle was kept similar to the one described above, and no post annealing was performed. The removal of this protective layer after SPS was ensured by either polishing or chemical etching in diluted phosphoric acid prior to microstructural and electrical characterizations (Figure 8c).

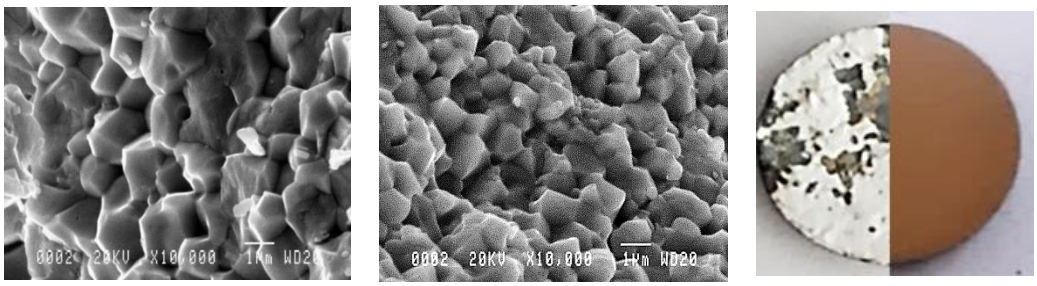

(**a**) (**b**) (**c**)

Figure 8. SEM images of fractured PZT ceramics sintered by spark plasma sintering (SPS) at 875 °C without a sintering aid: (**a**) Without a protective layer and (**b**) with $SrCO_3$. (**c**) Elimination of the $SrCO_3$ layer by etching or polishing.

PZT ceramics sintered without and with protective carbonate layers have an optimal relative density close to 98%, estimated by geometrical measurements. The microstructural investigation made on fractured ceramics revealed a homogeneous microstructure for all the ceramics with a comparable average grain size in the range 2–4 µm (Figure 8a,b). It can be concluded that the presence of a protective layer during SPS does not significantly affect the densification.

Electromechanical measurements performed directly after SPS with and without an annealing step are shown in Figure 9. Results with annealing were compared to those obtained with $SrCO_3$ and $BaCO_3$ as a protective layer. A slightly lower but comparable effective electromechanical coefficient k_{eff} was observed for samples with a $BaCO_3$ protective layer, with a value of ≈38%, whereas for $SrCO_3$, $k_{eff} \approx 40\%$.

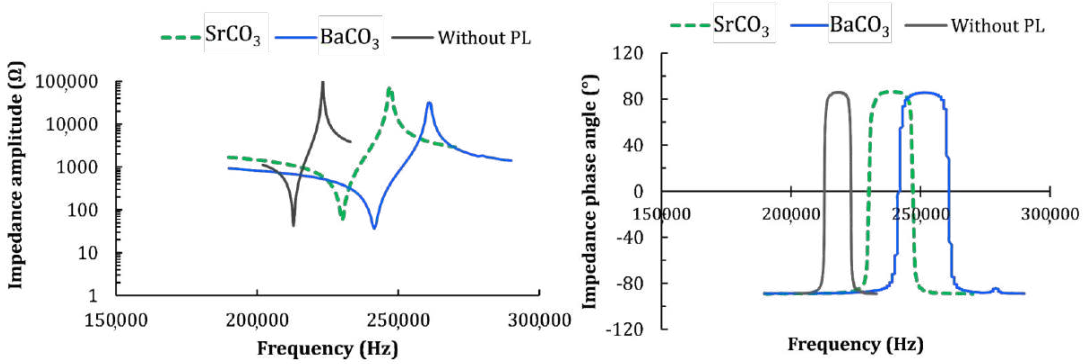

Figure 9. Comparison of impedance amplitude and impedance phase angle as a function of frequency for ceramics sintered by SPS with and without carbonates protective layers. Without PL refers to ceramics fabricated by SPS without a protective layer and post-annealed at 800 °C for 6 h.

These values are approaching those of a commercial PZ26 bulk ceramic ($k_{eff} \approx 50\%$) and remain appropriate for applications such as Structural Health Monitoring [30,31].

Despite a lower sintering temperature, 875 °C instead of 900 °C (screen-printed thick films) or 1200 °C (commercial ceramics), and the absence of additives, the electromechanical coupling factor reaches a good value, close to 40%. The room temperature relative dielectric permittivity at 1 kHz (not shown) for PZT sintered with $BaCO_3$ reaches 950 °C, a value lower than that obtained using $SrCO_3$ (i.e., 1500 °C). Relative densities are similar regardless of the nature of the protective layer, and a microstructural effect can be discarded to explain such a difference in permittivity values according to the nature of the protective layer used. However, a higher electric field can be applied to PZT ceramics when sintered with $BaCO_3$ compared to the PZT sintered with $SrCO_3$. This could explain the lower permittivity values when using $BaCO_3$. This could also reflect that $BaCO_3$ acts as a more efficient thermal barrier against diffusion and chemical reduction with a lower level of charged defects within the PZT as a result. Other effects such as electrode effects should be considered.

3.3. Towards Thick Films PZT Ceramic MEMS Sintered by SPS: Perspectives

3.3.1. Technical Adaptation

The good results obtained sintering thick films using a protective layer on one hand and bulk ceramics by SPS (Section 3.2) on the other lead to the ultimate stage of obtaining a complete thick-film-based MEMS by SPS in a single step. To do so, as in [42], the stack of layers (Au/PZT/Au) is first screen-printed on a stainless steel substrate, and the assembly is then sintered by SPS in one step.

Due to a more complex architecture, sintering MEMS multilayers present a certain number of issues to be mastered. Among them, the material's thermal expansion coefficients, interfaces, and delamination have to be considered for a reliable sintering/assembly.

The challenge is to avoid delamination between the active piezoelectric layer and the electrodes (bottom and/or top electrodes). This is mandatory to guarantee not only a viable process but also its reproducibility, as well as the polarization of the active material. The delamination between the different elements of the stack results from the concomitant contribution of mechanical (the thermal expansion coefficient (TEC)) and chemical effects (interdiffusion), making the optimization step quite difficult.

The high heating rates used in SPS have proved to minimize and even prevent the interdiffusion of chemical species and the formation of secondary phases and/or reaction fronts [63] while achieving high densification (98%). The uniaxial pressure applied during sintering is mandatory to ensure the assembly of the different elements of the stack and the densification while avoiding the flow or creep of the sample and minimizing the TEC effects. To do so on such a complex multilayer architecture, adaptation/modification of the basic graphite elements (graphite die) is mandatory.

Many examples of modified standard setups have already been reported for specific experiments [64–68]. Starting from the standard graphite die used in SPS experiments, the design of the graphite tools to be used was at first simplified to a "no die" setup with two Ø = 30 mm cylinders. The first direct advantage of this setup is the energy saving during heating, given the much lower graphite volume used compared with a classical complete die with the same inner diameter. The improved placement of the thermocouple for the temperature measurement (almost at the sample) allows for a much finer control of the sintering conditions. Finally, the configuration shown in Figure 10 allowed for the best results. A carbon element has been used in addition to the protective layer, in order to guarantee a minimum contact pressure during sintering to avoid delamination.

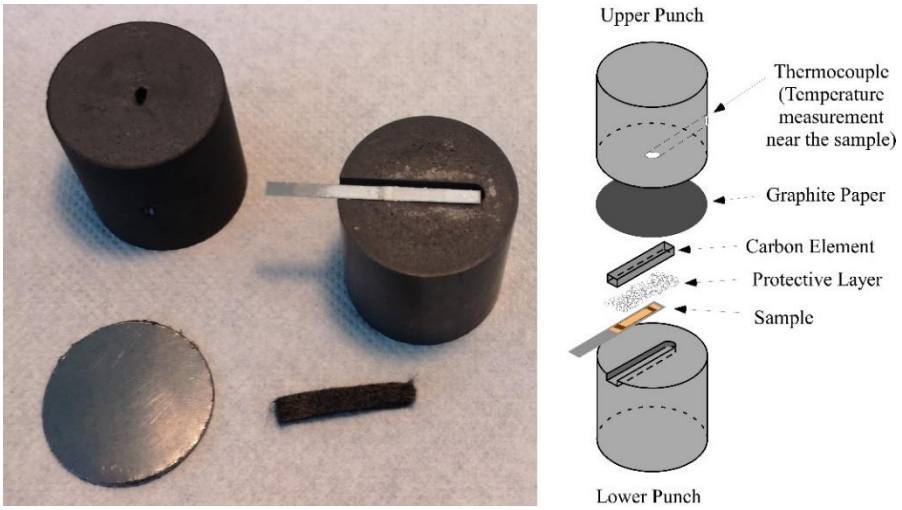

Figure 10. Final optimized configuration for the modified SPS graphite die.

A temperature of 850 °C was identified as the best for this setup, given the proximity of the thermocouple to the sample (a standard setup and a thermocouple at the surface of the die). The heating rate was set at 50 °C/min in all experiments performed under a primary vacuum, and a holding time of 5 min was fixed.

The microstructure of a fracture of the PZT within the multilayer obtained in the conditions described above was compared with that of the screen-printed PZT thick film conventionally sintered on the same stainless steel substrate (Figure 11). Grain sizes were comparable (≈1–4 µm), and in both cases the grain size distribution remained quite large. The level of porosity lay in the same range (15–20%), although in the case of SPS, the sintering temperature was slightly lower (850 °C versus 900 °C), and the sintering dwell time was significantly shorter (5′ instead of 2 h). In addition, it is noteworthy that SPS was performed without a sintering aid and without a preliminary pressure step. Compared to PZT ceramics sintered by SPS (Section 3.2), the increase in porosity within the

stack can be mainly explained by the low pressure applied on the multilayer and the slightly lower sintering temperature.

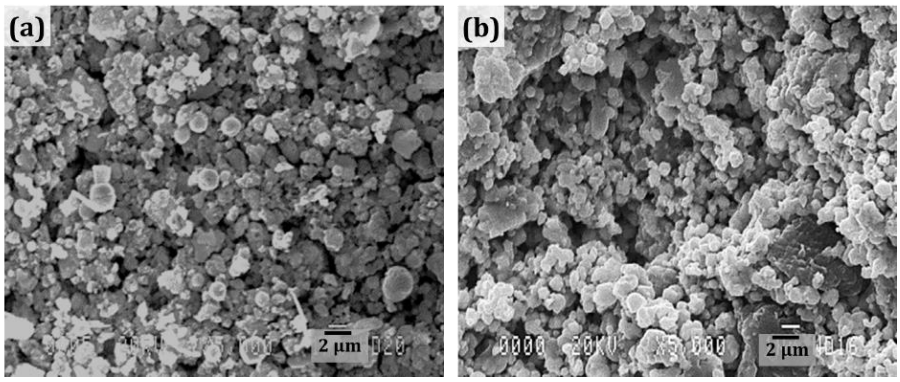

Figure 11. (a) SEM image of the active PZT layer within the Au/PZT/Au/SS sintered by SPS at 850 °C without sintering aid and (**b**) SEM image of screen-printed PZT thick film (900 °C, 2 h, sintering aid) [69].

3.3.2. Adaptation from the Point of View of Materials

Even if the optimization of the setup configuration is necessary, this aspect alone is not sufficient to reach the optimized densification of multilayers. Several preliminary tests have evidenced that the challenge in sintering the assembly relies more specifically on the control of the interfaces between the PZT and the electrodes (bottom and/or top electrodes). Delamination issues remain the main drawback, resulting in reduced conductivity, detrimental for piezoelectric properties. The key parameters to solve this problem do concern not only SPS set-up and parameter optimization but also the screen-printing process. Indeed the close link between temperature, mechanical constraints, and chemical reactivity during SPS depends on the nature and thickness of the different components, which need to be addressed even before the screen-printing process. Furthermore, the implementation of the sacrificial layer has to be considered when dealing with mechanical constraints and chemical reactivity. Thus, some lines of optimization can be highlighted, such as the nature of the protective layer, the substrate thickness, and the nature of the electrodes.

- Nature of carbonate protective layer

Previously, it was proved that highly densified ceramics with excellent properties can be obtained without a post-SPS annealing step using $SrCO_3$ or $BaCO_3$ as a protective layer. However, for multilayer structures, the choice of using $SrCO_3$ or $BaCO_3$ needs to be further studied. The carbonate can be removed after SPS by chemical etching according to the reaction given in Section 2.2 (Equation (1)). It has been observed that, when $SrCO_3$ is used, surface contamination (Sr content) on the sample remains even after the chemical attack (Figure 12). One difficulty compared to ceramics sintered by SPS using $SrCO_3$ is the fact that polishing the multilayer's surface (to remove surface contamination) is not possible without causing irreversible damages on the top gold electrode. Conversely, when using $BaCO_3$, the surface of the sample is not contaminated, and the layer can be more easily removed. This can be explained by the higher decomposition temperature (1350 °C) of $BaCO_3$ compared with $SrCO_3$ (Table 3) and, as a consequence, a higher stability in SPS conditions. $BaCO_3$ represents thus the most promising option to protect the active PZT layer from chemical reduction and thus to avoid a post–thermal treatment.

- Substrate thickness

One option to reduce temperature constraints arising mainly from the mismatch between thermal expansion coefficients is to reduce PZT or SS layer thicknesses. Reducing the PZT layer's thickness is not appropriate since it will directly affect the piezoelectric performance. Therefore, by reducing the SS substrate (initial thickness: 250 µm), delamination issues can be limited. Two different SS301 substrate thicknesses were studied: 25 µm and 100 µm. Samples were fabricated using the same thick-film and SPS process using $BaCO_3$ as a protective layer. Even if a good adhesion of the PZT layer was obtained, regardless of the thickness of the substrate (25 or 100 µm), further adaptation of the screen-printing process is required to guarantee a suitable quality of printing.

- Nature of electrodes

Au electrodes present good chemical compatibility with PZT, but Ag or Ag alloys are more attractive at an industrial level (reduced cost). Ag has great conductivity but is likely to migrate, and this can contribute to a failure of electric properties in PZT films. However, the presence of Pd, glass, or oxide additives in Ag-based ink can minimize this effect and can act as sintering aids for PZT, inducing a gain in densification and electrical properties at low co-firing temperature [24]. However, the experiments performed with a 250 µm substrate thickness using Ag/Pd electrodes did not show any improvement in adhesion (Figure 13a). Conversely, and as expected, samples with a 100 µm substrate thickness exhibited the best features in terms of interfaces within the multilayer (Figure 13b).

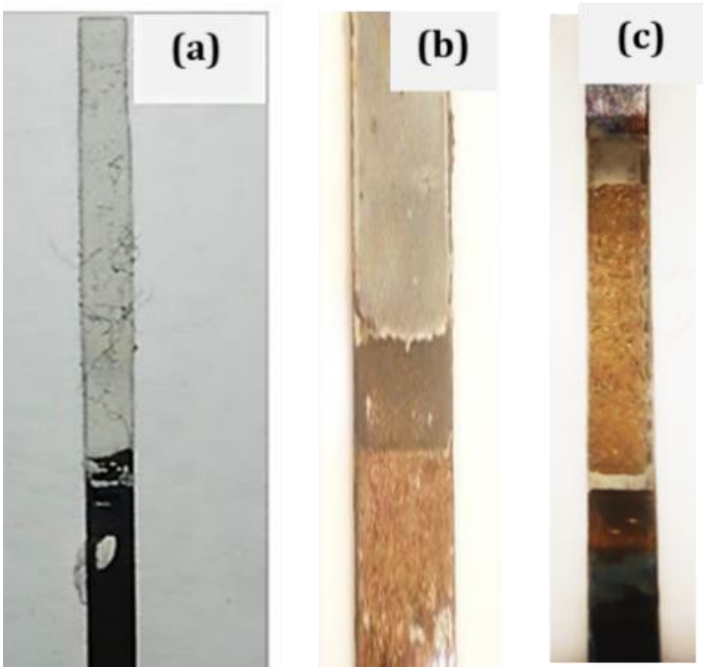

Figure 12. Comparison of multilayers after SPS using different natures of protective layers. (**a**) Samples after SPS for both $SrCO_3$ and $BaCO_3$. (**b**) Sample with $SrCO_3$ after chemical attack with H_3PO_4 showing the appearance of surface contamination (whitening on the top Au electrode). (**c**) Sample with a $BaCO_3$ protective layer after chemical removal.

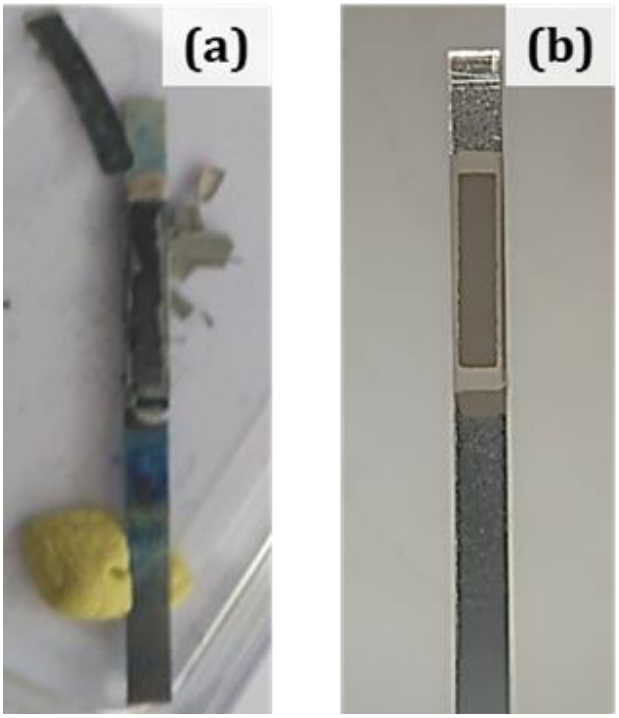

Figure 13. Samples obtained after SPS using Ag/Pd electrodes (**a**) with a 250 μm substrate thickness, resulting in destroyed samples, and (**b**) with a 100 μm substrate thickness, resulting in samples with good adhesion.

4. Conclusions

In many instances, sacrifice and protection are merged for the progress of complex systems, while keeping the environmental costs as low as possible. This very general law may apply to the processes reported here. In the search for advanced ceramics MEMS, we have recalled the use of different kinds of sacrificial layers for the fabrication of LTCC or thick-film MEMS. Stecher's work, more than 30 years ago, made it possible to initiate the realization of thick-film pressure sensors with cavities thanks to surface micromachining as for silicon MEMS. A carbon sacrificial layer was burnt out through a dielectric porous layer during the process. Processes using sacrificial layers have been continuously improved and in particular have extended towards the fabrication of piezoelectric thick-film or ceramic MEMS. To avoid long or aggressive procedures (hard chemical etching), mineral glass or gold sacrificial layers are no longer investigated. The carbon sacrificial layer has remained until today, and is mostly studied for piezoelectric MEMS, but PZT layers printed on a sacrificial layer based on polyester or corn starch have recently allowed for densification values close to those of a bulk PZT ceramic. Among the mineral-based layers, the use of strontium carbonate proved to be efficient and versatile for the implementation of MEMS based on different materials (glass, glass-ceramic, metals, PZT, etc.). Such a process is original because the mineral carbonate layer is retained during firing, supporting upper layers during sintering. The chemical attack of the carbonate at the end of the firing is soft and fast, without any damage of the MEMS. Even if carbonates ($SrCO_3$ or $CaCO_3$) used for thick-film MEMS or LTCC present some disadvantages such as constrained sintering or possible chemical reactivity with the active piezoelectric layers, they remain an element of choice because of their easy elimination.

Based on these considerations, a carbonate layer, which is very efficient in shaping free-standing piezoelectric resonators, has also been explored for designing ceramics and MEMS by SPS.

During the processing steps that require high temperatures, being able to control interdiffusion between metal electrodes and piezoelectric oxides and keep the electrode integrity, is a concern.

We have demonstrated that the same carbonate ($SrCO_3$ or $BaCO_3$) that is used as a sacrificial layer can be inserted to allow SPS at a low temperature and to protect the full stack against contamination.

Carbonate layers can thus be simultaneously sacrificial and protective. Moreover, thanks to their very broad stability range depending on their chemical content, carbonates can play this double role in many instances. Due to the recent extension of sintering tools towards low temperature densification, disposable oxides will be increasingly needed. Cold, hydrothermal, and SPS treatments have shown their ability to densify numerous compounds at unprecedentedly low temperatures. The integration of these compounds in actual devices may require sacrificial or protective layers that can be softly removed after processing. Based on our findings, carbonates fulfill most or all of these requirements.

Author Contributions: Conceptualization, H.D., C.E., and M.M.; methodology, S.G., M.-I.R.-T., O.S., U.-C.C., H.D., and C.E.; data curation, S.G., M.-I.R.-T., and O.S.; writing—original draft preparation, H.D., C.E., U.-C.C., and M.M.; supervision, H.D. and C.E.; writing—review and editing, H.D., C.E., and U.-C.C.; project administration, H.D. and C.E.; All authors have read and agreed to the published version of the manuscript.

Funding: This research received no external funding.

Acknowledgments: The authors would like to thank Laboratoire IMS and ICMCB for supporting part of this work, Utaiwan Watcharosin for TGA and DTG analyses (National Metal and Materials Technology Center, Thailand), and Pascale Garreta and Philippe Legros (Placamat-UMS 3626 CNRS-Université Bordeaux) for the SEM analysis.

Conflicts of Interest: The authors declare no conflict of interest.

References

1. Bhalla, S.; Moharana, S.; Talakokula, V.; Kaur, N. *Piezoelectric Materials: Applications in SHM, Energy Harvesting and Biomechanics*, 1st ed.; John and Wiley and Sons: Hoboken, NJ, USA, 2016.
2. Gatzen, H.; Saile, V.; Leuthold, J. *Micro and Nano Fabrication: Tools and Processes*; Springer: Berlin/Heidelberg, Germany, 2015.
3. Kanno, I. Piezoelectric MEMS: Ferroelectric thin films for MEMS applications. *Jpn. J. Appl. Phys.* **2018**, *57*, 040101. [CrossRef]
4. Akedo, J.; Park, J.H.; Kawakami, Y. Piezoelectric thick film fabricated with aerosol deposition and its application to piezoelectric devices. *Jpn. J. Appl. Phys.* **2018**, *57*, 07LA02. [CrossRef]
5. Kuscer, D.; Noshchenko, O.; Hana Uršič, H.; Malič, B. Piezoelectric Properties of Ink-Jet–Printed Lead Zirconate Titanate Thick Films Confirmed by Piezoresponse Force Microscopy. *Jpn. J. Appl. Phys.* **2018**, *57*, 7S1. [CrossRef]
6. Beeby, S.P. Printed thick-film mechanical microsystems (MEMS). In *Printed Films Materials Science and Applications in Sensors, Electronics and Photonics*; Prudenziati, M., Hormadaly, J., Eds.; Woohead Publishing: Cambridge, UK, 2012; pp. 259–277.
7. Stecher, G. Free supporting structures in thick-film technology: A substrate integrated sensor. In Proceedings of the 8th European microelectronics conference, Bournemouth, UK, 3–5 June 1987; pp. 421–427.
8. Stecher, G.; Spitzenberger, K.; Müller, K. Pressure Sensor. U.S. Patent 4,382,247, 3 May 1983.
9. Kok, S.L.; White, N.L.M.; Harris, N.R. Fabrication and characterization of free-standing thick-film piezoelectric cantilevers for energy harvesting. *Meas. Sci. Technol.* **2009**, *20*, 124010. [CrossRef]
10. Castille, C.; Dufour, I.; Lucat, C. Longitudinal vibration mode of piezoelectric thick-film cantilever-based sensors in liquid media. *Appl. Phys. Lett.* **2010**, *96*, 154102. [CrossRef]
11. Gongora-Rubio, M.R.; Espinoza-Vallejos, P.; Sola-Laguna, L.; Santiago-Avile, J.J. Overview of low temperature co-fired ceramics tape technology for meso-system technology (MsST). *Sens. Actuator A* **2001**, *89*, 222–241. [CrossRef]
12. Wei, Y.; Torah, R.; Yang, K.; Beeby, S.; Tudor, J. Screen printable sacrificial fabrication process to realise a cantilever on fabric using a piezoelectric layer to detect motion for wearable applications. *Sens. Actuator A* **2013**, *203*, 241–248. [CrossRef]
13. Rivadeneyra, A.; Fernández-Salmerón, J.; Agudo-Acemel, M.A.; López-Villanueva, J.; Fermín Capitan-Vallvey, L.; Palma, J.A. Improved manufacturing process for printed cantilevers by using water removable sacrificial substrate. *Sensor Actuator A* **2015**, *235*, 171–181. [CrossRef]

14. Nesser, H.; Ayela, C.; Dufour, I.; Debéda, H. Highly deformable printed organic trapezoidal micro-beams for vibration energy harvesting. *IOP Flex. Print. Electron.* **2017**, *2*, 015001. [CrossRef]
15. Dudina, D.V.B.; Bokhonov, B.B.; Olevsky, E.A. Fabrication of Porous Materials by Spark Plasma Sintering: A review. *Materials* **2019**, *12*, 541. [CrossRef]
16. Elissalde, C.; Chung, U.C.; Roulland, F.; Berthelot, R.; Artemenko, A.; Majimel, J.; Basov, S.; Piraux, L.; Nysten, B.; Mornet, S.; et al. Specific core-shell approaches and related properties in nanostructured ferroelectric ceramics. *Ferroelectrics* **2018**, *532*, 138–159. [CrossRef]
17. Debéda, H.; Rua-Taborda, M.I.; Chung, U.C.; Elissalde, C. One step densification of printed multilayer by SPS: Towards new piezoelectric energy harvester MEMS. In *Spark Plasma Sintering: Current Status, New Developments and Challenges*, 1st ed.; Cao, G., Estournes, C., Garay, R., Orrù, Eds.; Elsevier: Amsterdam, The Netherlands, 2019; pp. 219–255.
18. Maeder, T.; Yannick Fournier, Y.; Simon Wiedmer, S.; Hansu Birol, H.; Jacq, C.; Ryser, P. 3D Structuration of LTCC/Thick-film Sensors and Fluidic Devices. In Proceedings of the 3rd International Conference on Ceramic Interconnect and Ceramic Microsystems Technologies (CICMT), Denver, CO, USA, 23–26 April 2007.
19. Birol, H.; Maeder, T.; Ryser, P. Processing of graphite-based sacrificial layer for microfabrication of low temperature co-fired ceramics (LTCC). *Sens. Actuator A* **2006**, *130–131*, 560–567. [CrossRef]
20. Dai, X.; Yuan, Y.; Wei, T.; Tan, Q. Research on the Key Technology of LTCC Pressure Sensor. *Photonic Sens.* **2015**, *5*, 211–216. [CrossRef]
21. Fournier, Y.; Triverio, O.; Maeder, T.; Ryser, P. LTCC free-standing structures with mineral sacrificial paste. In Proceedings of the 4th International Conference on Ceramic Interconnect and Ceramic Microsystems Technologies (CICMT), Munich, Germany, 21–24 April 2008.
22. Lucat, C.; Ginet, P.; Castille, C.; Debéda, H.; Ménil, F. Microsystems elements based on free-standing thick-films made with a new sacrificial layer process. *Microelectron. Reliab.* **2008**, *48*, 872–875. [CrossRef]
23. Lucat, C.; Ginet, P.; Ménil, H.; Debéda-Hickel, H. Production of Multilayer Micro-Components by the Sacrificial Thick Layer Method. EUR. Patent Application No. 07712639.9, 25 April 2012.
24. Santawitee, O.; Grall, S.; Chayasombat, B.; Thanachayanont, C.; Hochart, X.; Bernard, J.; Debéda, H. Processing of printed piezoelectric microdisks effect of PZT particle sizes and electrodes on electromechanical properties. *J. Electroceramics* **2020**, *44*, 41–51. [CrossRef]
25. Grall, S.; Santawitee, O.; Dufour, I.; Aubry, V.; Debéda, H. New corn-based sacrificial layer for MEMS based on screen-printed PZT ceramics. *Sens. Actuators A Phys.* **2020**, *304*, 111826. [CrossRef]
26. Sippola, C.B.; Ahn, C.H. A thick film screen-printed ceramic capacitive pressure microsensor for high temperature applications. *J. Micromech. Microeng.* **2006**, *16*, 1086–1091. [CrossRef]
27. Ginet, P.; Lucat, C.; Ménil, F.; Battaglia, J.L. Modelling and Characterizing a Screen-Printed Metallic Electrothermal Microactuator. *Int. J. Appl. Ceram. Technol.* **2007**, *4*, 423–427. [CrossRef]
28. Lakhmi, R.; Debéda, H.; Dufour, I.; Lucat, C. Force sensors based on screen-printed microcantilevers. *IEEE Sens. J.* **2010**, *10*, 1133–1137. [CrossRef]
29. Debéda, H.; Lakhmi, R.; Lucat, C.; Dufour, I. Use of the longitudinal mode of screen-printed piezoelectric cantilevers coated with PEUT for toluene detection. *Comparison with silicon cantilevers. Sens. Actuators B Chem.* **2013**, *187*, 198–203. [CrossRef]
30. Debéda, H.; Lucat, C.; Maglione, M.; Pommier-Budinger, V.; Hochart, X.; Sourbe, W. Feasibility of screen-printed PZT microceramics for Structural Health Monitoring applications. *Int. J. Appl. Ceram. Technol.* **2014**, *11*, 413–421. [CrossRef]
31. Debéda, H.; Clément, P.; Llobet, E.; Lucat, C. One-step firing for electroded PZT thick-film s applied to MEMS. *Smart Mater. Struct.* **2015**, *24*, 025020. [CrossRef]
32. Ginet, P. Conception et Elaboration de Microstructures en Technologie Hybride Couche Epaisse Pour des Applications MEMS. Ph.D. Thesis, Electronic, Université Science and technology Bordeaux 1, Bordeaux, France, 2007.
33. Espinoza-Vallejos, P.; Zhong, J.; Gongora-Rubio, M.; Sola-Laguna, L.; Santiago-Aviles, J.J. The measurement and control of sagging in meso electromechanical LTCC structures and systems. In Proceedings of the MRS Conf. Proc., Boston, MA, USA, 30 November–4 December 1998; Volume 518, pp. 73–79.
34. Pranonsatit, S.; Lucyszyn, S. Self assembled screen-printed microwave inductors. *Electron. Lett.* **2005**, *41*, 23. [CrossRef]

35. Clément, P.; Perez, E.D.C.; Gonzalez, O.; Calavia, R.; Lucat, C.; Llobet, E.; Debéda, H. Gas discrimination using screen-printed piezoelectric cantilevers coated with carbon nanotubes. *Sens. Actuators B Chem.* **2016**, *237*, 1056–1065. [CrossRef]
36. Grall, S.; Dufour, I.; Aubry, V.; Debéda, H. Fabrication and characterisation of piezoelectric screen-printed in plane resonant microcantilevers used as gravimetric sensors. *Smart Mater. Struct.* **2019**, *28*, 105055. [CrossRef]
37. Beeby, S.P.; Blackburn, A. and White, N.M. Processing of PZT piezoelectric thick films on silicon for microelectromechanical systems. *J. Micromech. Microeng.* **1999**, *9*, 218. [CrossRef]
38. Xu, R.; Lei, A.; Dahl-Petersen, C.; Hansen, K.; Guizzetti, M.; Birkel, K.; Thomson, E.V.; Hansen, O. Screen printed PZT/PZT thick film bimorph MEMS cantilever device for vibration energy harvesting. *Sens. Actuators A Phys.* **2012**, *188*, 383–388. [CrossRef]
39. Ferrari, V.; Marioli, D.; Taroni, A. Theory, modeling and characterization of PZT-on-alumina resonant piezo-layers as acoustic-wave mass sensors. *Sens. Actuators A* **2001**, *92*, 182–190. [CrossRef]
40. Lou-Moeller, R.; Hindrichsen, C.C.; Thamdrup, L.H.; Bove, T.; Ringgaard, E.; Pedersen, A.F.; Thomsen, E.V. Screen-printed piezoceramic thick films for miniaturised devices. *J. Electroceramics* **2007**, *19*, 333–338. [CrossRef]
41. Lapeine, D.; Ferrandis, J.Y.; Oleksandr, F.; Fabien, P.; Combette, P. Study and optimization of screen-printed PZT transducers for acoustic applications. In Proceedings of the IEEE International Conference on Dielectrics (ICD), Montpellier, France, 3–7 July 2016.
42. Rua Taborda, M.I.; Elissalde, C.; Chung, U.C.; Maglione, M.; Fernandes, F.; Salehian, S.; Santawitee, S.; Debéda, H. Key features in the development of unimorph stainless steel cantilever with screen-printed PZT dedicated to energy harvesting applications. *Int. J. Appl. Ceram. Technol.* **2020**, *17*, 2533–2544. [CrossRef]
43. Pavlič, J.; Kosec, M.; Holc, J.; Rojac, T. K0.5Na0.5NbO3 thick films: Preparation and properties. In Proceedings of the 48th International Conference on Microelectronics, Devices and Materials, Otočec, Slovenia, September 19–September 21 2012.
44. Debéda, H.; Lucat, C.; Ménil, F. Influence of the densification parameters on screen-printed component properties. *J. Eur. Ceram. Soc.* **2005**, *25*, 2115–2119. [CrossRef]
45. Hindrichsen, C.G.; Lou-Moller, R.; Hansen, K.; Thomsen, E.V. Advantages of PZT thick film for MEMS sensors. *Sens. Actuators A Phys.* **2010**, *163*, 9–14. [CrossRef]
46. Lakhmi, R.; Debéda, H.; Dufour, I.; Lucat, C.; Maglione, M. Study of screen-printed PZT cantilevers both self-actuated and self-read-out. *Int. J. Appl. Ceram. Technol.* **2014**, *11*, 311–320. [CrossRef]
47. Wang, X.X.; Murakami, K.; Sugiyama, O.; Kaneko, S. Piezoelectric properties, densification behavior and microstructural evolution of low temperature sintered PZT ceramics with sintering aids. *J. Eur. Ceram. Soc.* **2001**, *21*, 1367–1370. [CrossRef]
48. Medesi, A.J.; Meier, H.; Megnin, C.; Hanemann, T. A novel Co-casting process for piezoelectric multilayer ceramics with silver inner electrodes. *Procedia Eng.* **2015**, *120*, 124–129. [CrossRef]
49. Kok, S.L.; Othman, R.; Shaaban, A. Screen-Printed Ceramic Based MEMS Piezoelectric Cantilever for Harvesting. *Adv. Sci. Technol.* **2014**, *90*, 84–92. [CrossRef]
50. Ferrari, V. Printed thick-film piezoelectric and pyroelectric sensors. In *Printed films, Prundenziati, M., Hormadaly, J., Eds.*; Woohead Publishing: Cambridge, UK, 2012; pp. 221–258.
51. Meggit Ferroperm TM Piezoceramics. Available online: https://www.meggittferroperm.com/wp-content/uploads/2017/10/Datasheet-hard-pz26.pdf (accessed on 2 August 2020).
52. Donnelly, N.J.; Shrout, T.R.; Randall, C.A. The Role of Li_2CO_3 and PbO in the Low-Temperature Sintering of Sr, K, Nb (SKN)-Doped PZT. *J. Am. Cerm. Soc.* **2009**, *92*, 1203. [CrossRef]
53. Bansal, N.P.; Bhalla, S.A.; Mahmoud, M.M.; Manjooran, N.J.; Singh, G.; Lamon, J.; Choi, S.R.; Pickrell, G.; Lu, K.; Geoff, B.; et al. *Ceramics Transaction. Processing and Properties of Advanced Ceramics and Composites IV*; Wiley: Hoboken, NJ, USA, 2014; Volume 249. [CrossRef]
54. Safar, M.; Button, T.W.; Zabcik, M. Control of PbO loss during sintering of PZT: Laboratory vs. industry. In Proceedings of the Joint IEEE International Symposium on the Applications of Ferroelectric (ISAF)/International Workshop on Acoustic Transduction Materials and Devices (IWATMD)/Piezoresponse Force Microscopy (PFM), Atlanta, GA, USA, 7–11 May 2017. [CrossRef]
55. Wang, D.; Guo, H.; Morandi, D.S.; Randall, C.A.; Trolier-McKinstry, S. Cold sintering and electrical characterization of lead zirconate titanate piezoelectric ceramics. *APL Mater.* **2018**, *6*, 016101. [CrossRef]

56. Legallais, M.; Fourcade, S.; Chung, U.C.; Michau, D.; Maglione, M.; Mauvy, F.; Elissalde, C. Fast re-oxidation kinetics and conduction pathway in spark plasma sintered ferroelectric ceramics. *J. Eur. Ceram. Soc.* **2018**, *38*, 543. [CrossRef]
57. Hu, Z.Y.; Zhang, Z.H.; Cheng, X.W.; Wang, F.C. A review of multi-physical fields induced phenomena and effects in spark plasma sintering: Fundamentals and applications. *Mater. Des.* **2020**, *191*, 108662. [CrossRef]
58. Grasso, S.; Sakka, Y.; Maizza, Y. Electric current activated/assisted sintering (ECAS): A review of patents 1906–2008. *Sci. Technol. Adv. Mater.* **2009**, *10*, 053001. [CrossRef]
59. Mercier, A.; Zehani, K.; Chaplier, G.; Pasko, A.; Loyau, V.; Mazaleyrat, F. Spark plasma sintering co-sintered monolithic transformers for power electronics. *IEEE Trans. Magn.* **2016**, *52*, 8400404. [CrossRef]
60. Radingoana, P.M.; Guillemet, S.; Olubambi, P.A.; Chevallier, G.; Estournès, C. Influence of processing parameters on the densification and the microstructure of pure zinc oxide ceramics prepared by spark plasma sintering. *Ceram. Int.* **2019**, *45*, 10035–10043. [CrossRef]
61. Manière, C.; Durand, L.; Weibel, A.; Chevallier, G.; Estournès, C. A sacrificial material approach for spark plasma sintering of complex shapes. *Scr. Mater.* **2016**, *124*, 126–128. [CrossRef]
62. Manière, C.; Nigito, E.; Durand, L.; Weibel, A.; Beynet, Y.; Estournès, C. Spark plasma sintering and complex shapes: The deformed interfaces approach. *Powder Technol.* **2017**, *320*, 340–345. [CrossRef]
63. Chung, U.C.; Elissalde, C.; Maglione, M.; Estournes, C.; Paté, M.; Ganne, J.P. Low losses, highly tunable $Ba_{0.6}Sr_{0.4}TiO_3$/MgO composite. *J. P. Appl. Phys. Lett.* **2008**, *92*, 042902. [CrossRef]
64. Anselmi-Tamburini, U.; Garay, J.E.; Munir, Z.A. Fast low-temperature consolidation of bulk nanometric ceramic materials. *Scr. Mater.* **2006**, *54*, 823–828. [CrossRef]
65. Bradbury, W.L.; Olevsky, E.A. Production of SiC–C composites by free-pressureless spark plasma sintering (FPSPS). *Scr. Mater.* **2010**, *63*, 77–80. [CrossRef]
66. Eqtesadi, S.; Motealleh, A.; Perera, F.H.; Miranda, P.; Pajares, A.; Wendelbo, R.; Guiberteau, F.; Ortiz, A.L. Fabricating geometrically-complex B4C ceramic components by robocasting and pressureless spark plasma sintering. *Scr. Mater.* **2018**, *145*, 14–18. [CrossRef]
67. Kwon, H.; Estili, M.; Takagi, K.; Miyazaki, T.; Kawasaki, A. Combination of hot extrusion and spark plasma sintering for producing carbon nanotube reinforced aluminum matrix composites. *Carbon* **2009**, *47*, 570–577. [CrossRef]
68. Morsi, K.; Esawi, A.M.K.; Borah, P.; Lanka, S.; Sayed, A.; Taher, M. Properties of single and dual matrix aluminum-carbon nanotube composites processed via spark plasma extrusion (SPE). *Mater. Sci. Eng. A* **2010**, *527*, 5686–5690. [CrossRef]
69. Rua Taborda, M.I. Printed Ceramic Piezoelectric MEMS for Energy Harvesting: Towards Spark Plasma Sintering of Multilayers. Ph.D. Thesis, Electronic, Université de Bordeaux, Bordeaux, France, 2019.